30 March 2001

ELSEVIER

Chemical Physics Letters 337 (2001) 107–116

CHEMICAL PHYSICS LETTERS

www.elsevier.nl/locate/cplett

Femtosecond coherence spectroscopy using spectrally selective differential photodetection

Florin Rosca, Dan Ionascu, Anand T.N. Kumar, Andrey A. Demidov, Paul M. Champion *

Physics Department and Center for Interdisciplinary Research on Complex Systems, 111 Dana Research Center, Northeastern University, Boston, MA 02115, USA

Received 14 November 2000; in final form 8 February 2001

Abstract

We present a novel, spectrally selective, detection scheme for pump–probe femtosecond coherence spectroscopy (FCS) that attenuates the non-oscillatory background signal so that the coherent oscillations are more clearly revealed. The method is based on spectral dispersion of the probe beam after it has traversed the sample, followed by detection of spectrally specific portions with a differential detector containing two balanced photodiodes. By appropriately choosing the spectral windows detected by each photodiode, we show how vibrational oscillations can be selectively enhanced or suppressed. Information about the phase behavior of the vibrational modes is also revealed using this detection scheme.

1. Introduction

Femtosecond coherence spectroscopy (FCS) is a pump–probe technique that utilizes the spectral bandwidth of femtosecond laser pulses to prepare and monitor coherent states in a wide variety of samples [1–10]. In this technique, a delayed probe pulse monitors the dynamic changes in sample absorption induced by a pump pulse. The two most common detection schemes [11,12] involve the detection of either the full bandwidth (open band) of the probe pulse, using a single photodiode, or the detection of a selected spectral window within the pulse bandwidth, using a monochromator and a photomultiplier tube (PMT) combination (dispersed detection). The measured signal is proportional to the imaginary part of the third-order polarization [10,13–16]. Polarization sensitive detection techniques such as optical heterodyne detection [10,13–16] have the ability to measure the real part of the tensorial third-order polarization (birefringent response) by using a local oscillator field that is $\pi/2$ out of phase with the probe field.

In the standard pump–probe experiment, coherent oscillations (associated with the nuclear vibrations) are often superimposed on a strong monotonically decaying background signal, especially for resonant samples. This background signal is usually related to processes like excited electronic state population decay, vibrational cooling, and ligand recombination (for samples that undergo photolysis, such as nitric oxide bound myoglobin [9] (MbNO)). The ability to

* Corresponding author. Fax: +1-617-373-2943.
E-mail address: champ@neu.edu (P.M. Champion).

0009-2614/01/$ - see front matter
PII: S0009-2614(01)00200-7

separate the oscillatory signals from the monotonically decaying background is particularly important for the detection of low frequency modes (<100 cm^{-1}). Unfortunately, it is often very difficult to experimentally extract the low frequency oscillatory signals from a strong background signal when using a typical open band detection scheme [1]. Neither the open band nor the dispersed detection methods outlined above can efficiently separate low frequency modes from the monotonic background. As a result, these oscillations are often extracted using numerical analysis techniques (e.g., linear predictive singular value decomposition (LPSVD)). In the current Letter, we demonstrate differential detection techniques that experimentally minimize the background signal by utilizing two photodiodes, which probe different spectral regions within the probe pulse spectral bandwidth. These methods can also be used to select and enhance a specific frequency range of coherent oscillations. As examples, we present experiments using both resonant (MbNO) and non-resonant (chloroform) samples.

2. Materials and methods

2.1. Pump–probe setup

The principal elements of femtosecond pump–probe laser setups are well known [12]. We use a self-mode-locked Ti:sapphire laser (MIRA 900, Coherent) pumped by a solid state cw laser (VERDI-V10, Coherent) to generate 45–120 fs light pulses with a center wavelength between 700 and 960 nm and repetition rate of 76 MHz. A 0.2 mm BBO crystal is used to double the optical frequency of these pulses. The average power of blue light at the sample is 30 mW, which corresponds to about 0.4 nJ per pulse pair. The pump–probe experiment utilizes a typical lock-in amplifier detection technique [18]. In the experiments reported here we used laser pulses centered at 439 nm for both the pump and probe beams. The novel part (see Fig. 1) of the experimental setup is at the probe detection stage. Here, we use a photodetector (Nirvana, New Focus) containing two photodiodes with a differential amplifier. A lock-in amplifier processes the differential signal because of the high signal-to-noise requirements needed to detect the coherent oscillations. Therefore, it is not possible to use a diode array detector, which would otherwise provide a more detailed measurement of the probe pulse spectral content.

We utilize two frequency selection methods. In the first one (Fig. 1a), we use a diffraction grating to wavelength disperse the probe beam after it passes through the sample and symmetrically split it into two parts (the red and blue sides). Each part is focused onto one of the differential detector photodiodes (see Fig. 1a). The differential output from the detector is then directed to the lock-in amplifier, which is synchronized at the pump chopping frequency (1.5 MHz). We abbreviate this method as BMR (blue-minus-red) detection. Obviously, if the signal detected by the blue-side photodiode has the same amplitude and phase (for oscillations) as that detected by the red-side photodiode, then the net result is zero. These conditions are satisfied for a monotonic background signal, which usually derives its sign and amplitude from the population dynamics of the photoexcited system. As a result, the BMR technique is effective at suppressing the background signal. On the other hand, coherent oscillations, which are also present in the detected signal, may have a significant change of their phases and amplitudes across the probe pulse spectrum [12–14,19]. Thus, the oscillatory signals can survive and even be enhanced by BMR detection.

In the second wavelength selection method (Fig. 1b), the central part of the spectrally dispersed probe beam (see Fig. 1c) is collected using a narrow mirror, such that the selected bandwidth contains half of the probe beam intensity (by adjusting the mirror angle and lens position), and is focused onto one of the photodiodes (PD2). The remaining light (in the spectral wings) (see Fig. 1b, c) is focused by another lens onto the other pho-

[1] We have also developed a wavelength selective modulation technique that uses a single photodiode, but multiple chopping frequencies to interrogate different parts of the pump and probe pulse spectral bandwidth. This technique is also able to suppress the population-induced background [17].

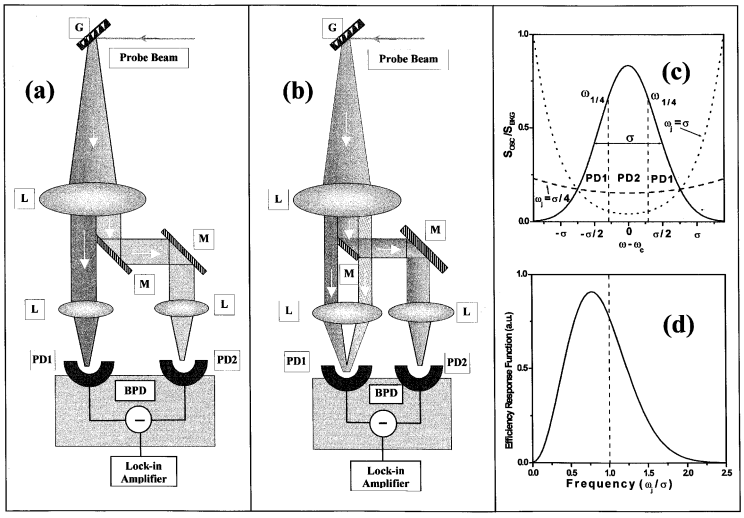

Fig. 1. Probe pulse detection using diffraction gratings and differential detector. The probe beam is dispersed by gratings (G) and different spectral regions are collected using mirrors (M) and lenses (L). The photodiodes PD1 and PD2 are connected to different arms of a differential balanced photodetector (BPD). The BPD is connected to a lock-in amplifier. Panel (a) shows BMR detection, and panel (b) shows WMC detection. (c) The dependence of the ratio of the oscillatory and background intensities for modes with frequencies equal to σ (dotted line) and $\sigma/4$ (dashed line). Here σ is the spectral bandwidth of the probe pulse. The two vertical dashed lines, labeled $\omega_{1/4}$ delineate the spectral wings (detected by photodiode PD2, Fig. 1b) from the central part (detected by photodiode PD1, Fig. 1b). (d) The calculated response function for the detection of a vibrational mode of frequency ω_j using the WMC method. For the calculation we used Eq. (8) in which the third-order polarization was considered through its proportionality to the displaced probe field: $P^{(3)} \propto I(\omega_j)[E(\omega-\omega_j)+E(\omega+\omega_j)]$, where the factor $I(\omega_j) \propto \exp(-(\ln 2)\omega_j^2/\sigma^2)$ is obtained by a convolution over the pump fields with an optical frequency difference of ω_j. In this estimation, we assume that the pulse bandwidth is narrow compared to the resonant absorption lineshape.

todiode (PD1). The differential output from the detector is then directed to the lock-in amplifier as in the BMR technique. We abbreviate this method as the WMC (wings-minus-center) technique. This method also suppresses background signal similar to the BMR method, but it affects the oscillatory signal differently compared with the BMR detection. Details will be discussed below.

2.2. Samples

The MbNO samples were prepared as described elsewhere [20]. The pump and probe laser wavelengths are chosen for resonant conditions with the well-characterized Soret absorption band of MbNO. As previously reported [12], the FCS signal from MbNO contains both monotonic background signal and coherent oscillations associated with nuclear vibrational modes. Thus, we use MbNO as an absorptive (resonant) sample in order to demonstrate the new techniques. For the experiments on non-resonant (transparent) samples we used chloroform, purchased from Sigma. Measurements were conducted using a ~3.5 in. diameter rotating sample cell with an optical path of 0.5 mm. The cell was rotated at ~4000 rotations per minute to refresh the sample in the illuminated volume. The pump pulse energy is ~0.4 nJ and we calculate that about 1% of the illuminated sample volume is photolyzed by each pulse. The absence of background when the probe precedes the pump demonstrates that the sample has completely reset before the arrival of the next pulse pair.

2.3. Data processing

The data were analyzed using a LPSVD algorithm [21,22]. This algorithm extracts the oscillatory parameters such as frequency, phase, amplitude and damping factors of the oscillations,

as well as the exponential decays of the non-oscillatory background. The extracted parameters for oscillations are used to construct the associated 'power spectrum', assuming Lorentzian lineshapes.

3. Theory

3.1. Theory development

In order to understand the details of the wavelength selection methods described below we first present some basic expressions used in the theory of FCS signal generation. The generic FCS signal for a delay time τ between pump and probe pulses can be expressed as follows [19]:

$$S(\tau) = \int_0^\infty \mathrm{d}\omega\, \omega \mathrm{Im}\left[E^*(\omega)P(\omega,\tau)\mathrm{e}^{-\mathrm{i}\omega\tau}\right], \tag{1}$$

where ω is the optical frequency, $E^*(\omega)$ is the complex conjugate of the probe pulse spectral field envelope and $P(\omega,\tau)$ is the third-order polarization [13–16]. For the present discussion, it is convenient to express $P(\omega,\tau)$ in terms of the two-frequency polarizability [23,24] $\alpha(\omega,\omega')$ as follows:

$$P(\omega,\tau) = \int_{-\infty}^{\infty} \mathrm{d}\omega'\, \alpha(\omega,\omega')E(\omega')\mathrm{e}^{\mathrm{i}\omega'\tau}. \tag{2}$$

The polarizability $\alpha(\omega,\omega')$ (tensor subscripts are omitted for convenience) is essentially a Fourier transform of the convolution of the third-order susceptibility tensor with two pump field interactions [23]. In the well-separated pulse (WSP) regime, the quantity $\alpha(\omega,\omega')$ may be viewed as describing the effective linear response of the non-stationary system created by the pump pulse [23,24]. If we consider a typical molecular system consisting of vibrational modes that are coupled to the electronic transitions, $\alpha(\omega,\omega')$ takes the following form (neglecting vibrational damping for simplicity):

$$\alpha(\omega,\omega') = \alpha_0(\omega)\delta(\omega-\omega') + \sum_j \alpha_j(\omega)\delta(\omega-\omega'\pm\omega_j), \tag{3}$$

where ω_j represents the mode frequency. The spectral function $\alpha_j(\omega)$ depends on the mode coupling strengths and electronic dephasing parameters in addition to the pump pulse characteristics that induce the mode displacements. Using Eqs. (2) and (3), it can be shown that the polarization $P(\omega,\tau)$ is proportional to a superposition of envelope functions $E(\omega\pm\omega_j)$ that are blue and red shifted from the spectral envelope of the incident probe field. Thus, resonances occur at frequencies $\pm\omega_j$ and correspond to coherent Stokes and anti-Stokes Raman scattering signals [13] (CSRS and CARS, respectively). It is clear that the resulting spectrally resolved signal (integrand of Eq. (1)) will be strongly dependent on the mode frequency as well as the pulse width (which defines the width of the spectral envelope). In particular, the background signal (i.e., the non-oscillatory part) exhibits very different behavior in spectrally resolved measurements compared to the oscillatory signals. The fact that $E(\omega)$ peaks at the carrier frequency ω_c, while $P(\omega)$ peaks at $\omega_c\pm\omega_j$ means that detuning from the carrier frequency can enhance the detection of high frequency modes.

The relative weight of the superposition of the CARS and CSRS components to the dispersed probe signal is highly sensitive to the frequency of excitation [19]. To illustrate this aspect, we plot in Fig. 2, the dispersed probe signal for a simple model system consisting of two optically coupled modes with frequencies 40 and 220 cm^{-1}. The absorption lineshape for the system is plotted in the top panel. Also shown is the spectral profile of the pulse used (duration 50 fs), for two values of the carrier frequencies near resonance (ω_{c1} and ω_{c2}) and for off-resonant excitation (ω_{c3}). We express the dispersed probe signal as

$$S(\omega,\tau) = A_j(\omega)\cos\left(\omega_j\tau+\varphi_j(\omega)\right), \tag{4}$$

where ω_j refers either to the 220 or the 40 cm^{-1} mode and ω is the detected optical frequency. In the lower panels of Fig. 2, we plot the detuning dependent amplitude $A_j(\omega)$ and the phase $\varphi_j(\omega)$ for all three carrier frequencies. When the carrier frequency is at the resonant maximum, the CARS and CSRS components are oppositely phased, so that their superposition gives a minimum at zero detuning. The integrated signal (open band detection) also vanishes at the resonant maximum. As we tune ω_c to the shoulders of the absorption

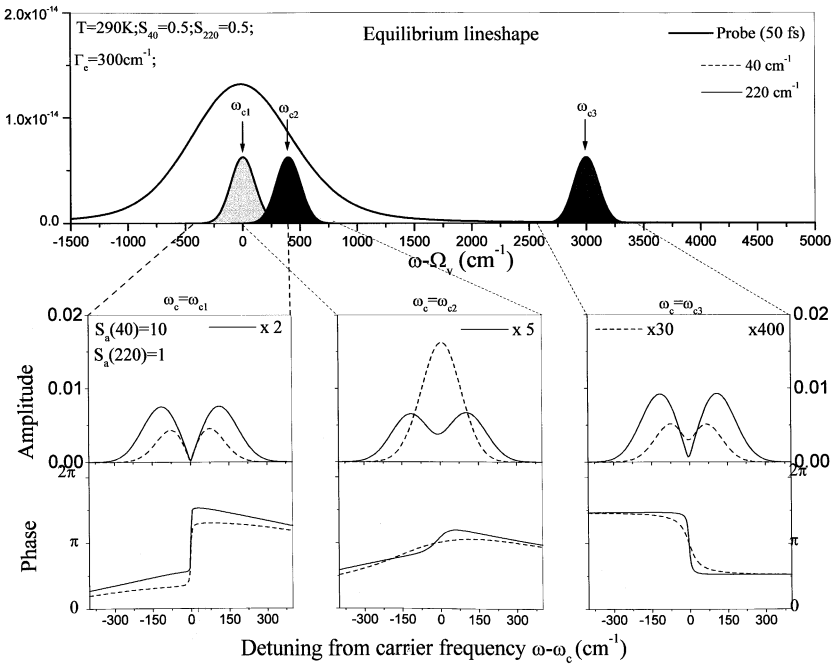

Fig. 2. The dispersed probe signal for a simple model system consisting of two optically coupled modes with frequencies 40 and 220 cm^{-1}. The absorption lineshape for the system is plotted in the top panel. Also shown is the spectral profile of the pulse used (duration 50 fs), for two values of the carrier frequencies near resonance (ω_{c1} and ω_{c2}) and for off-resonant excitation (ω_{c3}). The amplitude and phase behavior of the considered modes, 40 cm^{-1} (dashed line) and 220 cm^{-1} (solid line), is described in the lower panels for each of the three values of the carrier frequency.

spectrum, the CARS and CSRS components become more in-phase and begin to add constructively. The net result of the superposition is much stronger for the 40 cm^{-1} mode, as is evident from the figure. For off-resonant excitation, the CARS and CSRS components are again oppositely phased, corresponding to the fact that the integrated dichroic signal vanishes, as has been observed in transparent samples [13,14]. The highly detailed behavior of the dispersed signal depicted in Fig. 2 can be understood through the role played by the real and imaginary parts of the equilibrium lineshape functions, as detailed elsewhere [19]. For all the examples shown in the figure, we note that the 220 cm^{-1} mode is enhanced with detuning from ω_c.

3.2. BMR detection method

The theory described above is applicable to both the BMR and WMC detection methods, the only difference between them being the selection of the particular spectral windows that are detected by the photodiodes. We first consider the BMR detection method. The FCS signal generated using conventional detection techniques on resonant samples consists of an oscillatory part and a monotonically decaying background. In the BMR technique, the signals detected by the red and blue halves of the dispersed probe beam spectrum are subtracted from each other. Since the background signal is directly proportional to the intensity of the detected light, it is almost totally cancelled by the subtraction. If there is any residual background remaining, it is due to imperfect balancing of the photodiode outputs or to the weak wavelength dependence of the transient absorption signal across the spectral profile of the laser pulse. In contrast, the intensity of certain vibrational oscillations will not be suppressed, if they have a strong phase variation across the spectral bandwidth of the probe pulse [12]. Thus, the BMR

detection method is particularly useful for the observation of vibrational modes that display a strong phase variation as function of the detuning from ω_c. As seen in the lower panels of Fig. 2, such phase behavior is expected when ω_c is in resonance with the absorption maximum of the sample (ω_{c1}) as well as in off-resonant conditions (ω_{c3}).

3.3. WMC detection method

We now consider the WMC detection scheme and use Fig. 1c, d to describe it. The Gaussian spectrum of probe light (solid line) having a bandwidth σ is divided into three parts by the two dashed vertical lines (labeled $\omega_{1/4}$). The two spectral wings are detected on one photodiode (PD1) whereas the central part is detected on the second photodiode (PD2). This spectral selection is done such that the light intensity detected on the two photodiodes is equally distributed. Upon the subtraction of the signals generated by the two photodiodes, the background signal is greatly reduced. Again, the remaining background is mainly due to the weak wavelength dependence of the transient absorption signal (in this case, due to the second derivative of this signal) as well as to the imperfect balancing of the two photodiode outputs.

In order to understand the WMC detection method, we calculate the wavelength dependence of the ratio between the vibrational mode intensity and the background signal. For simplicity we assume that the carrier frequency is in a region with a slowly varying phase for the oscillatory signal, as well as a slowly varying sample absorption across the spectrum of the probe light. The phase behavior of the detected vibrational modes affects the WMC and the open band detection in a similar way. As discussed above, the background and oscillatory signal detected at a certain optical frequency (ω) depend upon the probe electric field in the following way:

$$S_{\mathrm{BKG}}(\omega) \propto |E(\omega)|^2, \tag{5}$$

$$\begin{aligned} S_{\mathrm{OSC}}(\omega,\omega_j) &\propto E(\omega)P^{(3)}(\omega,\omega_j) \\ &\propto E(\omega)\big[E(\omega-\omega_j)+E(\omega+\omega_j)\big], \end{aligned} \tag{6}$$

such that

$$\frac{S_{\mathrm{OSC}}(\omega,\omega_j)}{S_{\mathrm{BKG}}(\omega)} \propto \frac{E(\omega-\omega_j)+E(\omega+\omega_j)}{E(\omega)}, \tag{7}$$

where $E(\omega)=\exp[-2\ln 2(\omega-\omega_c)^2/\sigma^2]$ is the Fourier transform of the electric field with σ as the spectral full width at half maximum of the probe pulse and with ω_c as the carrier frequency. The frequency dependence of the ratio (Eq. (7)) is plotted in Fig. 1c for two vibrational modes of frequencies $\omega_j=\sigma$ (dotted line) and $\omega_j=\sigma/4$ (dashed line). The shape of these curves shows that the frequency dependence of the coherence signal and the background signal intensity are different (as clearly shown in Eqs. (5) and (6)). The oscillatory signal is more intense as one detunes away from the carrier frequency of the light and this effect is used to advantage in developing the WMC technique.

Applying Eq. (1) to the WMC detection scheme we obtain the following proportionality expression for the detection of a vibrational mode (ω_j):

$$\begin{aligned} S_{\mathrm{WMC}}(\omega_j) \propto & \int_{-\infty}^{-\omega_{1/4}} E(\omega)P^{(3)}(\omega,\omega_j)\,\mathrm{d}\omega \\ & - \int_{-\omega_{1/4}}^{+\omega_{1/4}} E(\omega)P^{(3)}(\omega,\omega_j)\,\mathrm{d}\omega \\ & + \int_{\omega_{1/4}}^{+\infty} E(\omega)P^{(3)}(\omega,\omega_j)\,\mathrm{d}\omega, \end{aligned} \tag{8}$$

where $-\omega_{1/4}$ and $\omega_{1/4}$ are the two wavelengths that delineate between the spectral regions detected on PD1 and PD2 (as seen in Fig. 1c). The effect of the finite pump bandwidth on the intensity of the generated modes is included in the expression of the third-order polarization, $P^{(3)}(\omega,\omega_j)$. The derived expression (Eq. (8)) defines the mode frequency dependent efficiency response function for the WMC detection scheme, which is plotted in Fig. 1d. We have used the variable ω_j/σ in the plot because σ is a directly accessible experimental quantity. One can see that for a given spectral bandwidth (σ) vibrational modes having frequencies near 0.75σ are maximally enhanced. Thus, we can conclude that for the observation of a 100 cm^{-1} mode using the WMC method, the optimal spectral bandwidth (σ) is about 133 cm^{-1}, which corresponds to a $\sim$110 fs transform limited pulse.

4. Results and discussion

4.1. Resonant samples

Fig. 3 demonstrates the application of the conventional open band detection and the BMR technique to MbNO using laser excitation at 439 nm. One can see (Fig. 3a) a strong background signal with low frequency oscillations superimposed on it. We have previously reported that for MbNO, the Fe-His mode (220 cm^{-1}) is triggered by NO photolysis [9] and that this mode has a π phase flip and a dip in intensity at around 439 nm [12]. The dip in the intensity is explained by the opposite phase of this mode, when detected in the red and blue halves of the laser pulse spectrum. This opposite phasing leads to intensity cancellation in the open band measurement at 439 nm. As a result, the Fe-His mode is not seen in the open band signal or the power spectrum (Fig. 3c) calculated from the LPSVD analysis. The dominating feature of the open band signal is a strong monotonic background with some low frequency modes, but without the Fe-His mode.

A dramatic change appears when, under the identical laser pulse and sample conditions, we apply the BMR detection technique (Fig. 3b, d). It can be seen that the background signal is greatly reduced and the Fe-His mode becomes the dominant feature in the data. The continued presence of the other low frequency modes in the detected signal is due to their incomplete cancellation, i.e., their phases must differ when detected in the blue and red halves of the probe spectrum. On the other hand, the disappearance of the 250 cm^{-1} mode (compare Fig. 3c, d) indicates a nearly constant phase behavior of this mode across the spectrum of probe light. This can occur for a ground state coherence, when the carrier frequency is properly detuned (e.g., see ω_{c2} in Fig. 2). Thus, the BMR method provides not only background free detection of vibrational modes, but it also allows one to derive valuable information about the phase behavior of the mode as a function of detection

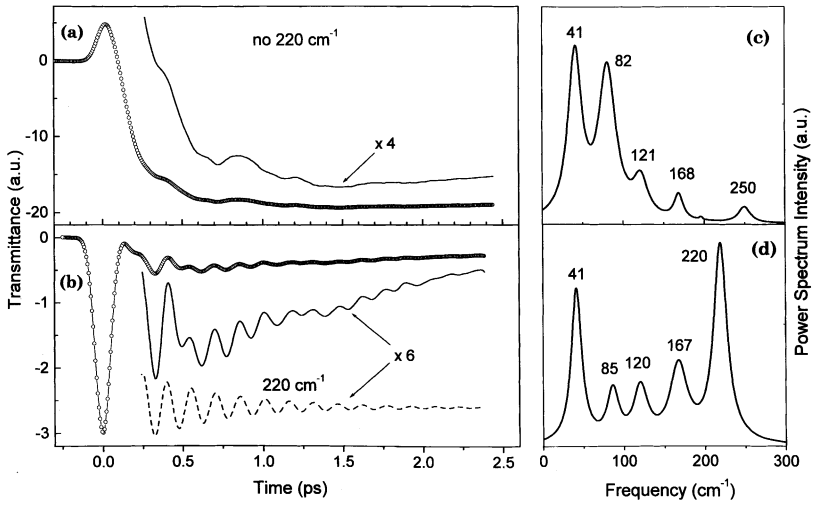

Fig. 3. The FCS signals from a sample of MbNO (a, b) and the associated power spectra (c, d). (a) The FCS open band signal detected using 439 nm laser pulses with a 250 cm^{-1} bandwidth. Circles are the experimental data, and the solid line represents the same data truncated, shifted and enlarged four times. (b) The FCS signal detected using 250 cm^{-1} bandwidth laser pulses and the BMR technique. The circles are the experimental data, and the solid line represents the same data truncated, shifted and enlarged six times. The displaced dashed line shows the 220 cm^{-1} mode used to fit the data. The residual background seen in the data is due to the small difference between the transient absorption signal detected by the red and blue halves of the probe spectrum, as well as due to slight imperfections in balancing the output of the two photodiodes. Panels (c) and (d) contain the respective power spectra calculated using parameters obtained from LPSVD analysis.

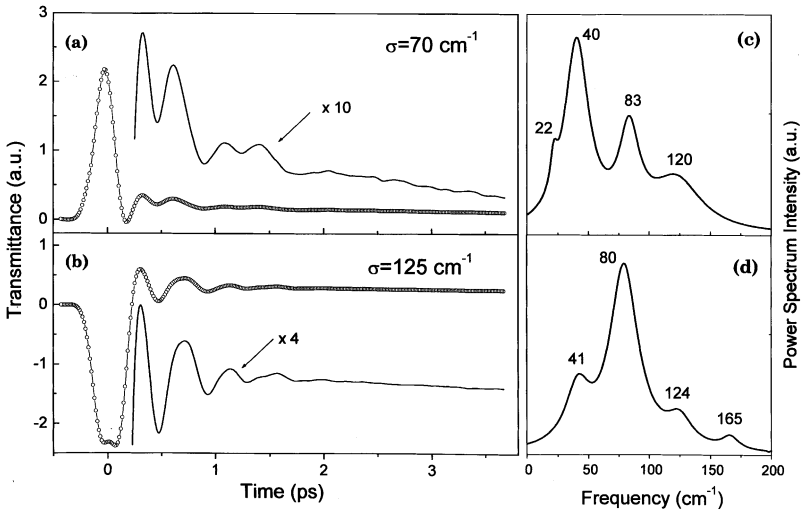

Fig. 4. The FCS signals from MbNO (a, b) measured with the WMC technique using laser pulses of 70 cm^{-1} (a) and 125 cm^{-1} (b) bandwidth, centered at 439 nm. Panels (c) and (d) show the associated power spectra found by LPSVD analysis. In panels (a) and (b) circles are the experimental data and solid lines represent the same data without the coherence spike, which are shifted and enlarged 10 (a) and 4 times (b).

frequency within the probe pulse spectrum. This can be helpful in assigning coherent features to their respective electronic states.

In Fig. 4 we demonstrate an application of the WMC technique to the same MbNO sample. We display the results of two experiments using different spectral bandwidth (σ) for the laser pulse. The FCS signals presented in this figure show a clear suppression of the monotonic background and the exposure of the low frequency oscillatory components. As expected (see Fig. 1d), Fig. 4 shows a significant enhancement of the 40 cm^{-1} mode for $\sigma = 70$ cm^{-1} (panel a), compared to the enhancement of the 80 cm^{-1} mode for $\sigma = 125$ cm^{-1} (panel b). For a more quantitative analysis, we compare the predicted intensity ratio of the two main observed modes (40 and 80 cm^{-1}) with the experimental values. For $\sigma = 70$ cm^{-1}, the theoretical value of I_{80}/I_{40} from Fig. 1d is 0.78 whereas the experimental measurement yields 0.62. For $\sigma = 125$ cm^{-1}, both the theoretical and the experimental values for I_{80}/I_{40} are 2.4. Thus, the data presented in Fig. 4 are in good agreement with the theoretical predictions given in Fig. 1d for the enhancement of vibrational modes as a function of mode frequency and spectral bandwidth (σ) of the probe pulse.

4.2. Non-resonant sample

The usual detection scheme for non-resonant samples utilizes either detuned detection with a monochromator and a PMT or an open band birefringent optical heterodyne detection technique [11,13]. The dichroic signal in transparent samples is very difficult to measure with open band detection because the CSRS and CARS parts of the signal cancel out, having opposite phases [13]. In Fig. 5 we present FCS results on chloroform measured in open band detection (horizontal dashed line with no signal observed), BMR detection (dotted line), and when only the blue part of the probe spectrum is detected (solid line). All signals are detected in the dichroic mode. The coherence spike around zero delay has been truncated to show the oscillatory signal more clearly. The inset shows the power spectrum for the BMR detected signal. The two observed modes (261 and 366 cm^{-1}) are Raman active and have been previously [11,13] observed using conventional techniques. Only the CARS part of the signal is detected when the blue half of the probe spectrum is selected. The BMR detection effectively adds the CSRS and CARS parts of the signal, generating a signal with double the intensity of that observed

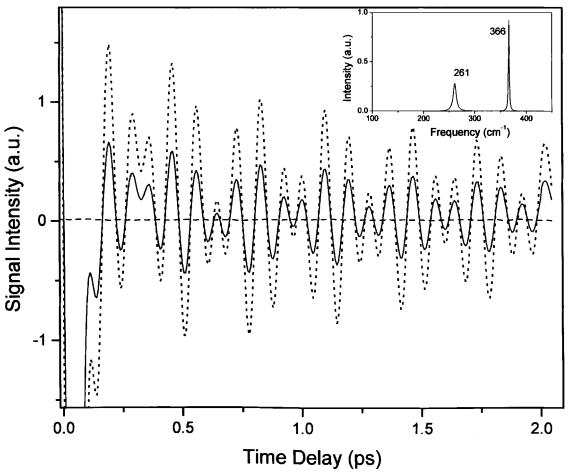

Fig. 5. The FCS signal obtained in chloroform using laser pulses having 250 cm^{-1} bandwidth and centered at 439 nm. The signal generated using open band detection is depicted as a horizontal dashed line. The signal generated by detecting only the blue half of the probe spectrum is depicted as a solid line. The results obtained using the BMR method are shown with a dotted line. The coherent spike is truncated to expose the oscillatory signals. The inset shows the power spectrum of the vibrational modes measured by the BMR method.

when only the blue half of the probe spectrum is detected.

5. Conclusions

We have presented a novel background-free detection technique for FCS experiments. The technique is based on the selection of different parts of the probe pulse spectrum and detection using two balanced photodiodes with a differential amplifier. The difference output signal carries the oscillatory signal, whereas the background is suppressed. These methods are especially useful in detecting low frequency vibrational modes in resonant samples, which are difficult to observe with conventional open band detection. We demonstrate that by using the WMC method, we can selectively enhance specific frequency regions by changing the spectral bandwidth of the laser pulse. For example, laser pulses having a 100 cm^{-1} spectral bandwidth are optimal for detecting a 75 cm^{-1} vibrational mode.

The BMR detection scheme allows one to explore the phase relations of the coherent vibrational signals across the spectrum of the probe laser pulse. The signals will either be suppressed or enhanced depending on the phase behavior in the blue and red parts of the laser pulse spectrum. For non-resonant samples, the BMR method allows one to easily extract reliable coherent oscillations of vibrational modes that are essentially undetectable using the standard open band (dichroic) measurement.

Acknowledgements

This work was supported by grants from NIH (DK-35090) and NSF (MCB-9904516).

References

[1] A.H. Zewail, Femtochemistry: Ultrafast Dynamics of the Chemical Bond, World Scientific, Singapore, 1994.
[2] M. Chachisvilis, H. Fidder, T. Pullerits, V. Sundstrom, J. Raman Spectrosc. 26 (1995) 513.
[3] M.H. Vos, F. Rappaport, J.C. Lambry, J. Breton, J.L. Martin, Nature 363 (1993) 320.
[4] N.F. Scherer, D.M. Jonas, G.R. Fleming, J. Chem. Phys 99 (1993) 153.
[5] J.C. Polanyi, A.H. Zewail, Acc. Chem. Res. 28 (1995) 119.
[6] N. Pugliano, A.Z. Szarka, R.M. Hochstrasser, J. Chem. Phys. 104 (1996) 5062.
[7] S. Ruhman, A.G. Joly, K.A. Nelson, J. Chem. Phys. 86 (1987) 6563.
[8] Q. Wang, R.W. Schoenlein, L.A. Peteanu, R.A. Mathies, C.V. Shank, Science 266 (1994) 422.
[9] L.Y. Zhu, J.T. Sage, P.M. Champion, Science 266 (1994) 629.
[10] L.D. Ziegler, R. Fan, A.E. Desrosiers, N.F. Scherer, J. Chem. Phys. 100 (1994) 1823.
[11] P.M. Champion, F. Rosca, W. Wang, A.T.N. Kumar, J. Christian, A. Demidov, Proc. SPIE in Laser Techniques for Condensed-Phase and Biological Systems 3273 (1998) 80.
[12] F. Rosca, A.T.N. Kumar, X. Ye, T. Sjodin, A.A. Demidov, P.M. Champion, J. Phys. Chem 104 (2000) 4280.
[13] S. Constantine, Y. Zhou, J. Morais, L.D. Ziegler, J. Phys. Chem. A 101 (1997) 5456.
[14] Y. Zhou, S. Constantine, S. Harrel, L.D. Ziegler, J. Chem. Phys 110 (1999) 5893.
[15] M.H. Cho, G.R. Fleming, S. Mukamel, J. Chem. Phys 98 (1993) 5314.
[16] M. Cho, M. Du, N.F. Scherer, G.R. Fleming, J. Chem. Phys 99 (1993) 2410.

[17] F. Rosca, A. Kumar, D. Ionascu, T. Sjodin, A. Demidov, P.M. Champion, J. Chem. Phys. (2001) in press.
[18] W. Wang, A.A. Demidov, X. Ye, J.F. Christian, T. Sjodin, P.M. Champion, J. Raman Spectrosc. 31 (2000) 99.
[19] A.T.N. Kumar, F. Rosca, A. Widom, P.M. Champion, J. Chem. Phys. 114 (2001) 701.
[20] S.Z. Hu, J.R. Kincaid, J. Am. Chem. Soc 113 (1991) 9760.
[21] H. Barkhuijsen, R. De Beer, W.M.M.J. Bovee, D. van Ormondt, J. Mag. Res. 61 (1985) 465.
[22] F. Wise, M. Rosker, G. Millhauser, C.L. Tang, J. Quantum Electron. QE-23 (1987) 1116.
[23] B. Fain, S.H. Lin, Chem. Phys. Lett 207 (1993) 287.
[24] B. Fain, S.H. Lin, Chem. Phys. 161 (1992) 515.